



HUBBLE SPACE TELESCOPE EXPANSION PARALLAXES OF THE PLANETARY NEBULAE NGC 6578, NGC 6884, NGC 6891, AND IC 2448¹

STACY PALEN AND BRUCE BALICK

Department of Astronomy, University of Washington, Physics/Astronomy Building, Stevens Way, Box 351580,
Seattle, WA 98195-1580; palen@astro.washington.edu, balick@astro.washington.edu

ARSEN R. HAJIAN

US Naval Observatory, 3450 Massachusetts Avenue, NW, Washington, DC 20392-5420; hajian@usno.navy.mil

YERVANT TERZIAN

Department of Astronomy, Cornell University, 512 Space Sciences Building, Ithaca, NY 14853-6801; terzian@astrosun.astro.cornell.edu

AND

HOWARD E. BOND AND NINO PANAGIA²

Space Telescope Science Institute, 3700 San Martin Drive, Baltimore, MD 21218; bond@stsci.edu, panagia@stsci.edu

Received 2001 December 20; accepted 2002 January 22

ABSTRACT

We have combined two epochs of *Hubble Space Telescope* WFPC2 imaging data with ground-based expansion velocities to determine distances to three planetary nebulae (NGC 6578, NGC 6884, and IC 2448). We used two variants of the expansion parallax technique—a gradient method and a magnification method—to determine the distances. The results from the two methods agree to within the errors. A fourth nebula was included in the study (NGC 6891), but the expansion was too small to determine the distance, and only a lower limit was obtained. This is the second paper in a series that will examine at least 24 nebulae in total.

Key words: planetary nebulae: general

1. INTRODUCTION

Few planetary nebulae (PNs) in our Galaxy have accurately determined distances. This has hampered our ability to use PNs as distance indicators in other galaxies and has limited the accuracy of derived PN properties, which are strongly dependent on distance, such as luminosity or nebular mass. Even the spatial distribution of PNs in the Milky Way is poorly determined, leading to uncertainties in the total number of PNs and the birth rate. Because PN progenitors are sources of carbon and nitrogen, the PN population strongly influences the chemical evolution of the galaxy as a whole (see, e.g., Martins & Viegas 2000). In particular, these progenitors contribute to the chemical evolution of carbon in the interstellar medium (e.g., Iben 1985; Palla et al. 2000).

Most PN distances have been derived statistically and are accurate only when taken as a whole (not for individual members of the population). Prior to 1995, statistical distance scales relied on an assumption of a universal physical property such as the ionized nebular mass, luminosity of the central star, or uniform extinction along the line of sight. These assumptions often introduce large errors. For example, PNs are formed from progenitor stars with masses ranging over an order of magnitude, all of which shed enough mass to drop to between ~ 0.5 and $1 M_{\odot}$ during the PN phase. These statistical scales generally gave results accurate to a factor of 2 at best for individual targets (see, e.g., Shklovskii 1956; O'Dell 1962; Daub 1982; Maciel & Pottasch 1980; Cahn, Kaler, & Stanghellini 1992). See

Terzian (1993) for a review of the difficulties inherent in finding distances to PNs.

More recently, Zhang (1995) devised two additional statistical methods to determine distances to PNs, based on empirically determined relationships between the ionized mass and the radius of the object (mass-radius relation) and between the radio continuum surface brightness and the radius (surface brightness-radius relation). Using both of these relations, he claims an accuracy of $\sim 35\%$ – 50% . These distances are still not sufficiently accurate to enable a solution to several different PN problems. In part, the poor accuracy of the statistical distances is a result of calibration to a small sample of nearby PNs with distances that have been determined by other means. Most recently, several efforts have been underway to improve this nearby sample.

Trigonometric parallax has been used in recent years to find the distances to PNs, as CCDs have improved the astrometric measurements. Harris et al. (1997) report distances to 11 PNs accurate to 20%, and a further five with distances accurate to 50%, all from ground-based trigonometric parallax. The *Hipparcos* satellite measured parallax distances to a small sample of PNs, most to less than 50% accuracy (Acker et al. 1998). Pottasch & Acker (1998) compared these distances to previously determined spectroscopic distances to three PNs and found that the parallax distances were all much smaller than the spectroscopic distances. Gutierrez-Moreno et al. (1999) found ground-based trigonometric parallaxes for three objects and determined that there was no correlation between the previously determined statistical distances and the distances that they find from this fundamentally direct method. They do find, however, that distances determined from other methods, such as expansion parallax or sodium absorption, are highly correlated with their results. They interpret this as a fundamental failing of the statistical methods.

¹ Based on observations with the NASA/ESA *Hubble Space Telescope*, obtained at the Space Telescope Science Institute, which is operated by AURA, Inc., under NASA contract NAS 5-26555.

² On assignment from the Research and Scientific Support Department of the European Space Agency.

Ciardullo et al. (1999) have used the *Hubble Space Telescope* (*HST*) to discover close companions of the central stars of PNs. They used main-sequence photometric parallax to derive reliable distances to nine objects with companions. Distances to a further three objects are given in that paper, but the association of the binary pair is less certain. Bond & Ciardullo (1999b) also reported a ground-based distance to NGC 246 based on photometry of the resolved binary companion.

Expansion parallax distances have been determined using the Very Large Array (VLA) for eight PNs (Masson 1989a, 1989b; Gomez, Rodriguez, & Moran 1993; Hajian, Terzian, & Bignell 1993, 1995; Hajian & Terzian 1996). These distances are precise to roughly 10%–20% in some cases, provided that the assumptions of elliptical morphology and constant expansion velocity are correct. Lower limits on about six more objects have been determined using this method.

The high spatial resolution offered by *HST* makes it potentially very useful for determining expansion parallaxes of PNs. Prior to the work described in this paper, Reed et al. (1999, hereafter Paper I) have used *HST* to determine the distance to one PN, NGC 6543, using the expansion parallax method.

The expansion parallax method relies on the assumption that the expanding nebula is a prolate ellipsoid. Then the minor-axis expansion velocity in the plane of the sky (V_m) is related to the line-of-sight velocity (V) at the position of the central star. In the case of complex nebulae, such as point-symmetric or extremely bipolar nebulae, the method fails. Fortunately, if a nebula is close enough that V_m is observable over a few years, it is also close enough that the morphology may be accurately determined.

We also assume in this method that the spectroscopy and the imaging are sampling the same physical regimes within the object. It is possible that the angular expansion shows the motion of the ionization front, while the radial velocity measures the bulk motion of the gas. This will lead to an underestimate of the distance to the nebula.

A second assumption is that the nebula has been expanding at the same velocity for the elapsed time over which the parallax is being measured. The VLA and *HST* have sufficient angular resolution and fidelity to measure an expansion in just 4 yr. It is unlikely that the expansion speed of the nebular gas will be dramatically altered in this short period of time.

The distance is given by the small-angle formula

$$D = \frac{V_m}{\dot{\theta}}, \quad (1)$$

where V_m is the expansion velocity of the emitting material on the minor axis relative to the central star and $\dot{\theta}$ is the angular expansion of the radius of the nebula as measured on the sky. Converting to convenient units gives

$$D_{\text{pc}} = 211 \frac{V_m (\text{km s}^{-1})}{\dot{\theta} (\text{mas yr}^{-1})}. \quad (2)$$

Expansion velocities are derived from Doppler shifts along the line of sight to the central star, corrected for geometric projection effects.

We determined the angular expansion of the nebulae from the V -band *HST* images with two techniques: the gradient method and the magnification method, both described below. In this paper we report the direct measurement of

expansion parallax distances to three nebulae. In § 2 we describe the observations and the data reduction, including the alignment of the *HST* images. In § 3 we describe the three-dimensional modeling technique used to determine the ratio of the line-of-sight velocity to the velocity along the minor axis. In § 4 we describe in more detail the methods for finding the angular expansion of the nebula and discuss the pros and cons of each method. In §§ 5–8 we discuss the results and derived properties for each of the four PNs. Finally, in § 9 we discuss possible sources of systematic errors and future plans for the application of the methodologies described here.

2. OBSERVATIONS

2.1. Imaging with *HST*: Wide Field Planetary Camera 2

This paper describes results specifically for NGC 6578, NGC 6884, NGC 6891, and IC 2448. The first-epoch observations of these objects were obtained in a V -band (F555W filter) Wide Field Planetary Camera (WFPC2) snapshot survey by Bond & Ciardullo (1999a; Cycle 5, GO program 6119). The target objects were placed in the center of the planetary camera (PC) chip. Because this survey was optimized for observations of central stars, it was carried out in the broad V band, rather than in a nebular emission line. Thus, comparison to the radial velocities obtained from [O III] spectroscopic data must be done with some care. However, since [O III] is almost always the main contributor to the V -band flux from PNs, comparing V -band imaging with [O III] spectroscopy will not be a problem. Other possible contributions to the V band come from H β , He I ($\lambda\lambda 4921, 5015, 5876$, and weaker lines), and usually negligible contributions from various Fe and N lines, as well as the nebular continuum (which will contribute more to the V -band image than to the [O III], since the spectral window is wider).

From the survey of Bond & Ciardullo (1999a), we chose the 24 most spherically symmetric objects and reobserved many of them with WFPC2 on *HST* in Cycles 8 and 9. NGC 6578, NGC 6884, NGC 6891, and IC 2448 are the first four objects with second-epoch images. In the second epoch, we obtained [O III] (F502N) and [N II] (F658N) data in addition to new V -band images. In some cases, the [N II] images allow us to investigate in more detail complementary nebular volumes and speculate about the nebular evolution. Table 1 summarizes the imaging observations.

TABLE 1
Hubble Space Telescope OBSERVATIONS

Object	Date	Filters	Durations (s)	δT (yr)
NGC 6578.....	1995 Aug 16	V	70	4.2
	1999 Oct 23	V , [O III], [N II]	70, 460, 800	
NGC 6884.....	1995 Oct 13	V	80	4.0
	1999 Oct 22	V , [O III], [N II]	80, 560, 800	
NGC 6891.....	1995 Nov 20	V	3	3.9
	1999 Oct 22	V , [O III], [N II]	3, 360, 640	
IC 2448.....	1995 Oct 10	V	16	4.0
	1999 Oct 07	V , [O III], [N II]	16, 360, 1050	

2.1.1. Imaging Calibrations

Cosmic rays were removed using the IRAF task *crrej*. Correction for optical camera distortions was performed with the IRAF/STSDAS task *drizzle* (Fruchter & Hook 2002) with the Trauger coefficients. After these corrections, the chief problem was aligning images from different epochs properly. Despite our best efforts to repeat the first-epoch observations exactly, the images from the two epochs were not quite perfectly aligned. These small errors could be due to a number of effects, such as proper motions of guide stars or drifts in the instruments. Translations of fewer than 5 pixels in each direction and rotations of a few tenths of a degree were required to register the two epochs in each case. Such translations are not important unless the optical distortion corrections are in error; even so, they are not likely to produce a false-positive expansion for the entire nebula.

Using IDL, we made a first-order translation correction by aligning the images relative to a “pivot” star. We found the centroids and determined the offsets between epochs in the x -direction (δx) and y -direction (δy) by subtracting these coordinates.

We then chose three stars in each image, found the centroids in the two epochs [(x_1, y_1) and (x_2, y_2)], and solved for the rotation required to align the first image with the second,

$$\theta_{\text{rot}} = \arctan\left(\frac{y_1 - \delta y}{x_1 - \delta x}\right) - \arctan\left(\frac{y_2}{x_2}\right). \quad (3)$$

We compared the three values of θ_{rot} from the three stars, to check for discrepancies due to proper motion, geometric distortions, or other complicating factors. If the agreement was good, the three results were averaged to determine the rotation between the two images. If the agreement was bad, three new stars (or a new pivot) were chosen, and the process was repeated.

Finally, the translation of the images relative to the central star of the nebula was determined. For the case of an overexposed central star, we located the star by fitting lines to each of the diffraction spikes (which make an “X” on the image), rather than just finding the centroid.

To apply the transformations, the image from the first epoch was magnified by a factor of 10, the translations were applied, and the image was demagnified to its original size. (IDL allows only shifts of integer pixel size and uses a bilinear interpolation when magnifying and neighborhood averaging when demagnifying.) The second-epoch image was magnified, rotated, and demagnified. Then the two images were subtracted and the alignment visually inspected. The point-spread function is rotated, and so the stars never subtract completely. We used the nebula itself to check the alignment, looking for patterns of offsets that could result from a shift between one epoch and the next. This could result from, for example, proper motions of the background stars. If necessary, one image was “nudged” relative to the other, with these small translations further improving the alignment.

To check that we are not introducing significant errors in this process, we applied two tests. First, we transformed the final images back and subtracted from the originals. The residuals were small in all cases (less than 4% when integrated across the entire nebula) and appeared mainly in places where the nebula was faint and close to the level of the noise in the images. Second, we applied the rotation to

TABLE 2
SPECTROSCOPIC OBSERVATIONS

Object	Date	Location	Exposure (s)	V (km s ⁻¹)	$V_{\text{lit}}^{\text{a}}$ (km s ⁻¹)
NGC 6578.....	1999	CTIO	70	19.2 ± 0.5	...
NGC 6884.....	1999	KPNO	80	16.6 ± 0.4	23
NGC 6891.....	1999	KPNO	3	7.7 ± 0.8	7
IC 2448.....	1999	CTIO	16	17.9 ± 0.3	13.5

^a For convenience, V_{lit} is also given for some objects. These literature velocities are taken from Weinberger 1989, which tabulates results from several different studies.

the first-epoch image and the translation to the second-epoch image and subtracted the resulting difference map from the difference map derived above. Again, there was good agreement. This method of aligning the images results in only small artifacts, due mainly to the interpolations carried out when regridding the data near undersampled features.

2.2. Spectroscopy

High spectral resolution echelle data were obtained from the 4 m telescopes at Kitt Peak and the Cerro Tololo Inter-American Observatory (CTIO). In both cases, the cross-disperser was replaced with a mirror, so that only one order, centered around [O III], was obtained. The instrument resolution was 0.06 Å pixel⁻¹ (3.7 km s⁻¹), and a narrowband interference filter was used (~70 Å). Errors in the expansion velocity obtained from [O III], a strong line in all cases, are of order 10%. The spectroscopic observations are summarized in Table 2.

2.2.1. Spectroscopy Calibrations

The echelle spectra were bias-subtracted and flat-fielded. Thorium-Argon lamp spectra were used to solve for geometric distortions by iteratively using the IRAF tasks *identify*, *reidentify*, *fitcoords*, and *transform*. In some instances, we used skylines in the images to test the accuracy of these corrections. There were no significant deviations at the 0.1 pixel level. These lamp spectra were also used to calibrate the wavelength scale. The expansion velocity along the line of sight to the central star was found from these data by fitting Gaussians to the double-peaked velocity profile, subtracting the velocities of the peaks, and dividing by 2.

3. MODELING

The nebula is assumed to be a pinched oblate ellipsoid inclined to the line of sight (see Fig. 1). It is assumed to be expanding ballistically, so that the ratio of the axes is equal to the ratio of the velocities along those axes:

$$\frac{r_p}{r_m} = \frac{v_p}{v_m}, \quad (4)$$

where r_p and v_p are the radius and velocity along the long (polar) axis and r_m and v_m are the radius and velocity along the short (minor) axis. Then, the ratio of the line-of-sight velocity, V , to the true minor-axis velocity, v_m , is given by

$$\alpha = \frac{V}{v_m} = 1 + \left(\frac{r_p}{r_m} - 1\right) |\cos^n \phi|, \quad (5)$$

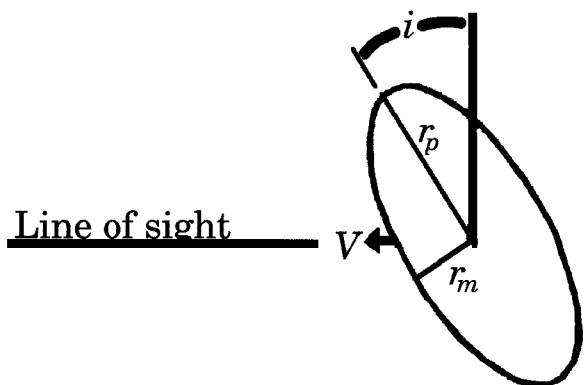


FIG. 1.—Oblate ellipsoid inclined to the line of sight: v is the observed velocity, r_p is the semimajor axis, r_m is the semiminor axis, and i is the inclination angle.

where ϕ is the azimuthal angle and n is functionally a shape parameter, defining how sharply the “waist” is pinched.

We derive n , r_p/r_m , and the inclination angle from code written in IDL that simulates a ballistically expanding pinched-waist elliptical nebula. Once this nebula is created, a “slit” is placed across it and a velocity spectrum derived, similar to that observed in the echelle. Both the projected nebula and the spectrum are overplotted on the observed data, and the parameters are varied manually until the shapes of the data are recovered. Because we have two sets of echelle data, one along the short axis and one along the long axis, the parameters are uniquely determined once a set of values is found that matches the image and both spectra. The fits to each nebula are shown in Figures 3–6 below, and the derived parameters are given in Table 3. These derived parameters are used to determine the true velocity along the minor axis from the line-of-sight velocity:

$$v_m = \frac{V}{\alpha} \tag{6}$$

4. DETERMINING THE ANGULAR EXPANSION

4.1. The Gradient Method

In the simplest case, when a nebula expands self-similarly, a difference image (epoch 2 – epoch 1) shows a bright outline surrounding a dark outline. When the expansion is resolved, features may expand through several pixels, and the distance between the peak and the trough of the difference map will give the angular expansion. When the expansion is unresolved, features move through less than a pixel. If the flux is high, we can still find the angular expansion by dividing the difference in the flux (δf) by the gradient (df/dr), thus recovering the angular expansion (δr). Dividing this angular expansion by the time elapsed gives an expansion rate. This

TABLE 3
MODEL-DERIVED PARAMETERS

Object	P.A. (deg)	V_p/V_m	i (deg)	n	V_m (km s ⁻¹)
NGC 6578.....	180, 270	1.3	25	0.9	15.1 ± 0.5
NGC 6884.....	111, 200	1.6	40	1.5	11.86 ± 0.4
NGC 6891.....	220, 310	1.5	35	6	6.70 ± 0.8
IC 2448	135, 215	1.3	25	3	14.67 ± 0.3

TABLE 4
GRADIENT DATA

Object	V_m (km s ⁻¹)	$\dot{\theta}$ (mas yr ⁻¹)	Distance (kpc)
NGC 6578.....	15.1 ± 0.5	1.95 ± 1.0	1.63 ± 1.07
NGC 6884.....	11.9 ± 0.4	1.60 ± 1.0	1.56 ± 0.98
NGC 6891.....	6.7 ± 0.8
IC 2448	14.7 ± 0.3	2.19 ± 1.0	1.41 ± 0.64

method gives two estimates for the angular expansion, one at either end of the minor axis. This method is described in greater detail in Hajian et al. (1993).

Operationally, we used IDL to make these measurements. After choosing a cut along the minor axis, we overplot the flux measurement along that axis and the derivative (df/dr). Using these plots, we can find the difference in the flux and the derivative at the location of the peak, and therefore the angular expansion. This is done several times, for each end of the minor axis, and the average value is reported in Table 4. Errors in this method are found from the standard deviation of these measurements.

4.2. The Magnification Method

Following Paper I, we also determined the angular expansion of a nebula by magnifying the first-epoch image by a factor, M , and subtracting it from the second. The process was repeated for a reasonable range of M ($1 < M < 1.2$), to find the value of M that minimized the residuals. This method assumes that the entire nebula expands at the same rate, but since we do not require the entire nebula to disappear when we subtract the magnified epoch but rather search for an M that gives the best fit to the second-epoch image, the effect of this assumption is minimized. The angular expansion rate of the radius is given by

$$\dot{\theta} = \frac{(M - 1)\theta}{\delta T} \tag{7}$$

where θ is the angle between the center of the nebula and the bright rim being used to determine the best fit and δT is the time elapsed between epochs of observation. This method shows graphically how the nebular expansion varies from the assumed uniform expansion. Errors are found by comparing the difference images at various magnifications. The largest step for which there is no observable change between difference images is taken as the accuracy of the measurement. For example, if $M = 1.001$ and 1.002 yield indistinguishable difference maps, but $M = 1.0025$ is obviously different from both, then the error in the measurement is 0.001. (The error is determined in both directions, i.e., in the preceding example, the difference map at $M = 1.0005$ is also distinguishable from the difference maps at $M = 1.001$ and 1.002 .) Table 5 summarizes the magnification results.

5. NGC 6578

5.1. Morphology

Figure 2 shows a color composite of the [N II], [O III], and V-band images. All of these are images from the second epoch. In the V-band image, NGC 6578 exhibits a bright

TABLE 5
MAGNIFICATION DATA

Object	V_m (km s^{-1})	Magnification	θ (mas)	$\dot{\theta}$ (mas yr^{-1})	Distance (kpc)
NGC 6578.....	15.1 ± 0.5	1.002 ± 0.0005	3359 ± 90	1.6 ± 0.4	2.00 ± 0.5
NGC 6884.....	11.86 ± 0.4	1.002 ± 0.0005	2275 ± 90	1.14 ± 0.3	2.20 ± 0.8
NGC 6891.....	6.7 ± 0.8
IC 2448	14.67 ± 0.3	1.002 ± 0.0005	4500 ± 90	2.25 ± 0.6	1.38 ± 0.4

central core ($\theta = 6''3$), surrounded by a fainter halo (about $11''$ in diameter). The inner core appears to have two “blow-out” bulbs along a single axis passing through the central star, from slightly west of north to slightly east of south.

These blowout lobes are colocated with halo regions of decreased brightness. Perhaps these are places where the inner core is not confined as tightly by the halo as the rest of the core.

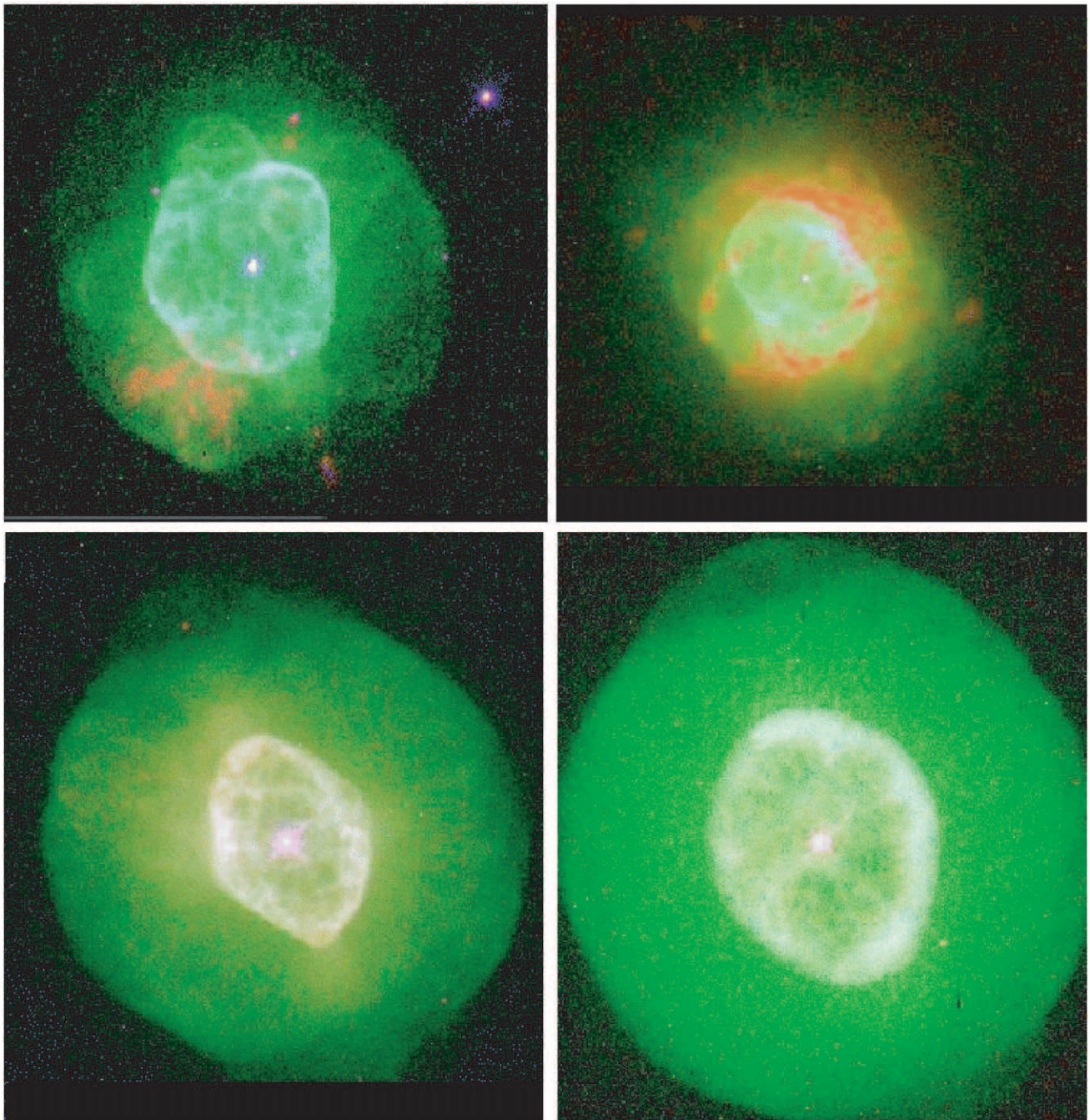


FIG. 2.—Color composites of V -band, [N II], and [O III] emission from each nebula. [N II] is red, [O III] is green, and V is blue

In the [N II] second-epoch image, there are a few bright knots that seem to be associated with the southeast blowout region. Two of these knots are very close together and may be physically connected. All of these knots appear to have downstream “tails,” which point away from the central star and away from the blowout region, similar to those in the Helix Nebula, but with many fewer knots.

Along a second axis, approximately from east to west, is a much larger [N II] emission axis, with the lower [N II] emission region containing many approximately spherical blobs of [N II] emission. None of these knots appear to have tails of the type exhibited by the southeast knots. This may be an orientation effect, or it may be real—there is no “blowout” appearance along this axis. The outer edge of this set of blobs is sharply bounded. The diffuse [N II] emission also appears to drop to zero at approximately the same location. While the diffuse emission extends from the central core to the outer edge of the blobs, the [N II] blobs appear to be entirely exterior to the bright inner core.

The inner core has a bright rim and a blotchy inner appearance, reminiscent of a heap of soapsuds, with faint regions surrounded by bright rims. These bright rims appear to be outlines, not striations. They do not in general cross each other, but where one rim is perpendicular to another, they make a “T.” We may be viewing a tightly

packed bundle of smaller hollow bubbles. When viewed in projection, they give this blotchy appearance.

The inner core of this nebula appears to be a waisted ellipsoid with axial ratio 1.3 : 1 and an inclination angle of 25° (see Table 3). However, the inner core is quite asymmetric, and this is the poorest fit of all the nebulae studied here.

5.2. Distance/Size Determination

The time between observations of NGC 6578 was 4.2 yr. Figure 3*d* is the difference image from the epoch subtraction in *V* band, and Figures 3*a*, 3*b*, and 3*c* are the *V*-band, [O III], and [N II] images, respectively. These *V* and [O III] images show a strong correspondence, implying that the kinematic [O III] expansion can be compared to the angular expansion measured in *V*. The echelle spectrum of [O III] gives a line-of-sight expansion velocity of $19.2 \pm 0.5 \text{ km s}^{-1}$.

The gradient method (as always, along the minor axis) yields an angular expansion rate of $1.95 \pm 1.0 \text{ mas yr}^{-1}$, corresponding to a distance of $1.63 \pm 1.07 \text{ kpc}$. The magnification method gives a magnification factor of 1.002 ± 0.0005 , which corresponds to an angular expansion rate of $1.6 \pm 0.4 \text{ mas yr}^{-1}$ and a distance of $2.00 \pm 0.5 \text{ kpc}$.

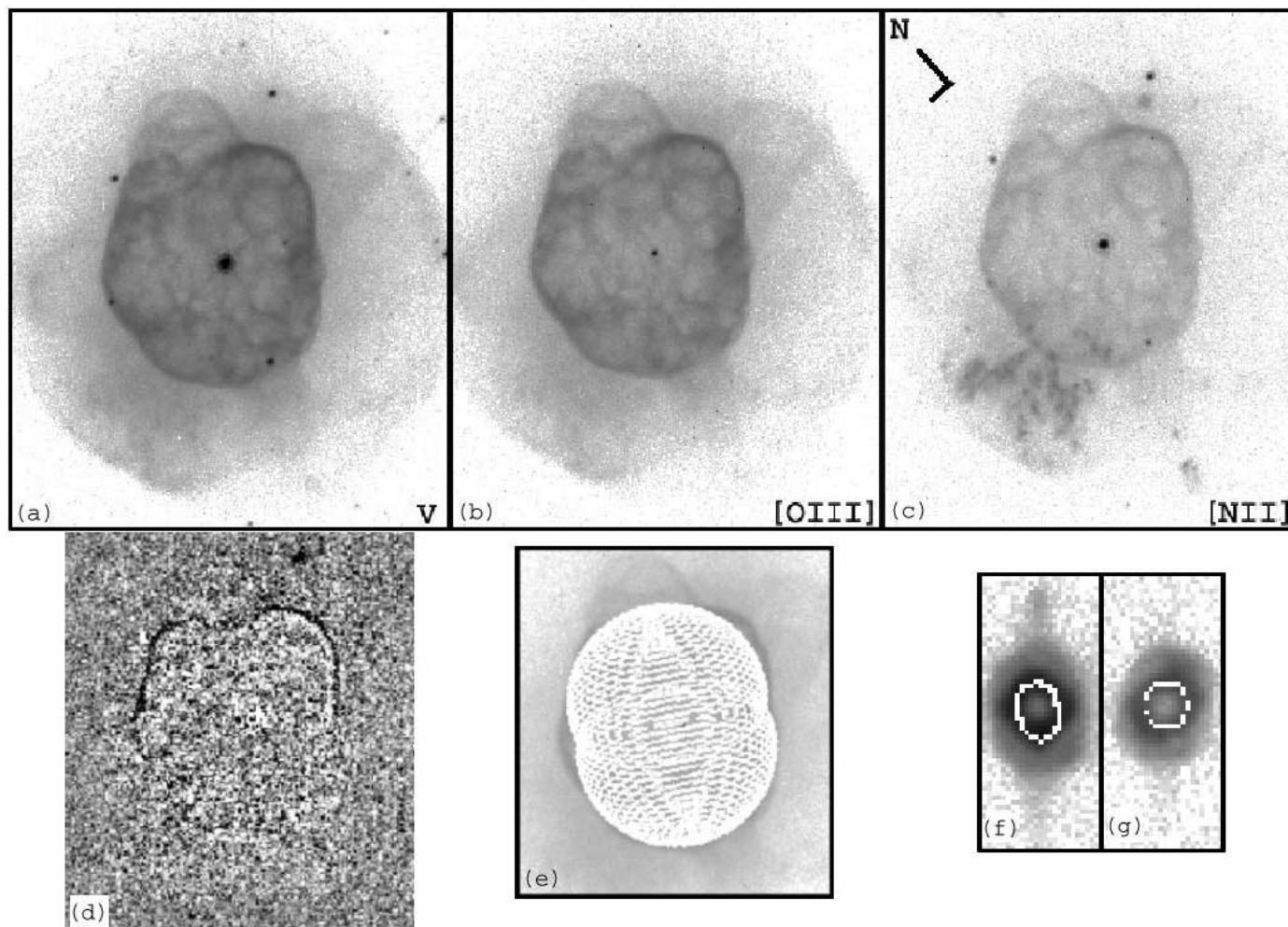


FIG. 3.—Observations of and model fits to NGC 6578: (a) original epoch 2 *V*-band image; (b) [O III] image; (c) [N II] image; (d) difference of the two *V*-band images taken 4.2 yr apart; (e) waisted ellipsoid fit to the image; (f) fit to P.A. = 180° ; (g) fit to P.A. = 270° .

6. NGC 6884

6.1. Morphology

Figure 4 shows the image data for this object. This nebula has an “S-shaped” inner core, point-symmetric around the central star, similar to NGC 7009. This inner core is surrounded by a filamentary region, perhaps a round ring inclined at an angle of approximately 45° . This is in excellent agreement with the 40° inclination angle derived from the model of this nebula. Outside this ellipse is faint [O III] emission, which appears to be constrained to regions perpendicular to the ring.

Quite puzzling, but typical of point-symmetric bipolars, is the presence of faint [N II] blobs disconnected from the inner nebula (see the red “blobs” in Fig. 2). There are two of these, extending along an axis quite different from any of the other symmetry axes in the nebula, at P.A. = 135° . Unfortunately, our kinematic data were taken along P.A. = 111° and 200° , and so we have no kinematic information to further investigate whether these blobs might be FLIERs.

The inner core of this nebula is fitted very well by a prolate ellipsoid with axial ratio 1.6 : 1 and an inclination angle of 40° . The nebula is quite symmetrical and therefore well described by this elliptical model.

6.2. Distance/Size Determination

A total of 4 yr elapsed between observations of NGC 6884. Figure 4 shows the image data. Again, the [O III] images are a good match to the *V*-band data (Fig. 4), so we are confident that comparing [O III] velocities with *V*-band expansions is reasonable. The echelle data for this nebula indicate a line-of-sight expansion velocity of $16.6 \pm 0.4 \text{ km s}^{-1}$.

The gradient method expansion velocity of this nebula is $1.6 \pm 1.0 \text{ mas yr}^{-1}$, which gives a distance of $1.56 \pm 0.98 \text{ kpc}$. Using the minor axis of the central core to determine the magnification gives an angular expansion velocity of $1.14 \pm 0.3 \text{ mas yr}^{-1}$. This corresponds to a distance of $2.2 \pm 0.8 \text{ kpc}$.

7. NGC 6891

7.1. Morphology

This nebula has an elliptical inner core (see Fig. 5), with an irregular outer halo. This is in distinct contrast with the other three nebulae, where the outer halo is symmetrical and the inner core is irregularly shaped. In detail, the inner core is fairly irregular, with brighter filaments crossing the surface. These filaments may have the same structure as the filaments in NGC 6578, but they are fainter in this nebula,

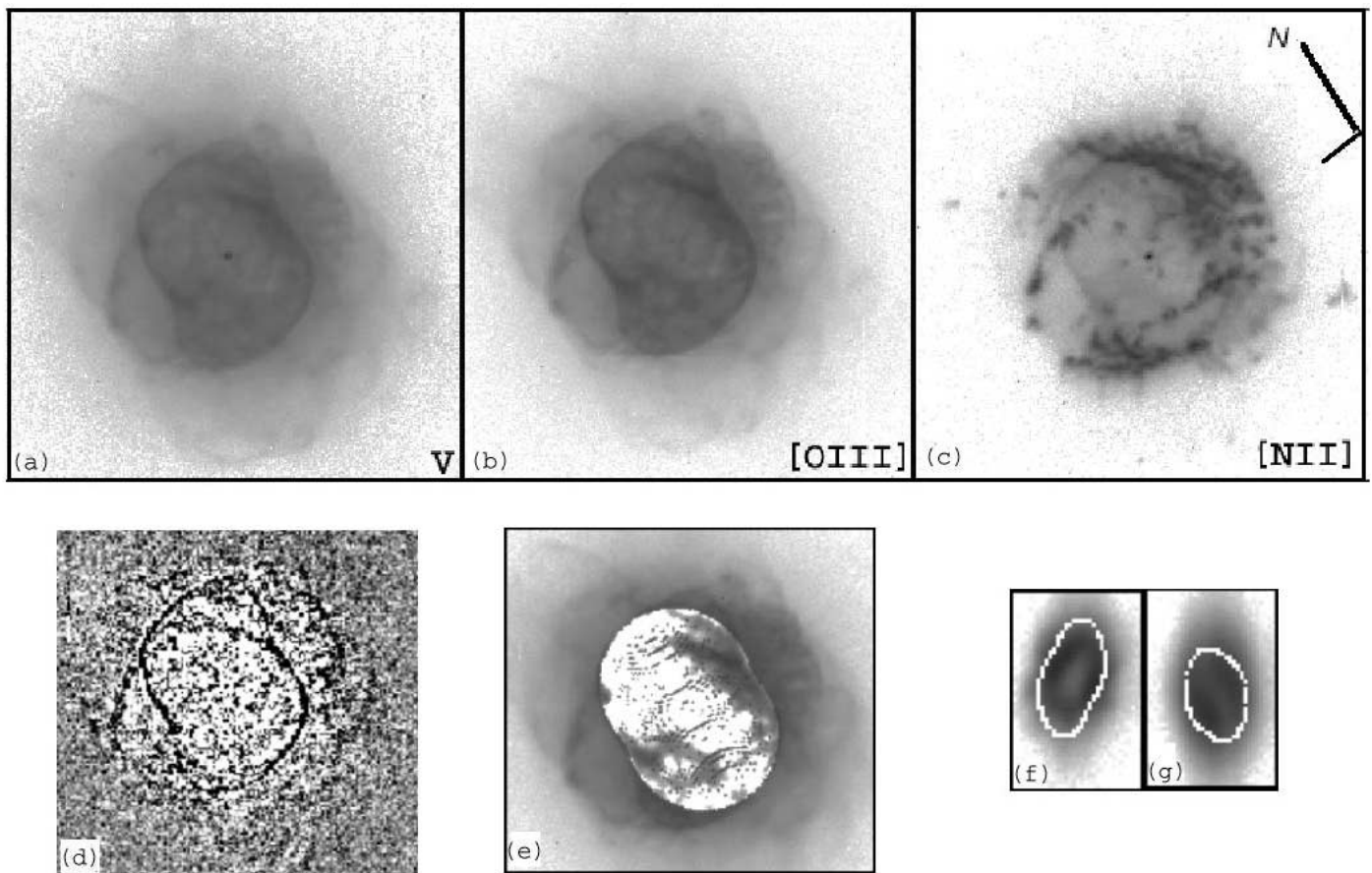


FIG. 4.—Observations of and model fits to NGC 6884: (a) original epoch 2 *V*-band image; (b) [O III] image; (c) [N II] image; (d) difference of the two *V*-band images taken 4.0 yr apart; (e) waisted ellipsoid fit to the image; (f) fit to P.A. = 111° ; (g) fit to P.A. = 200° .

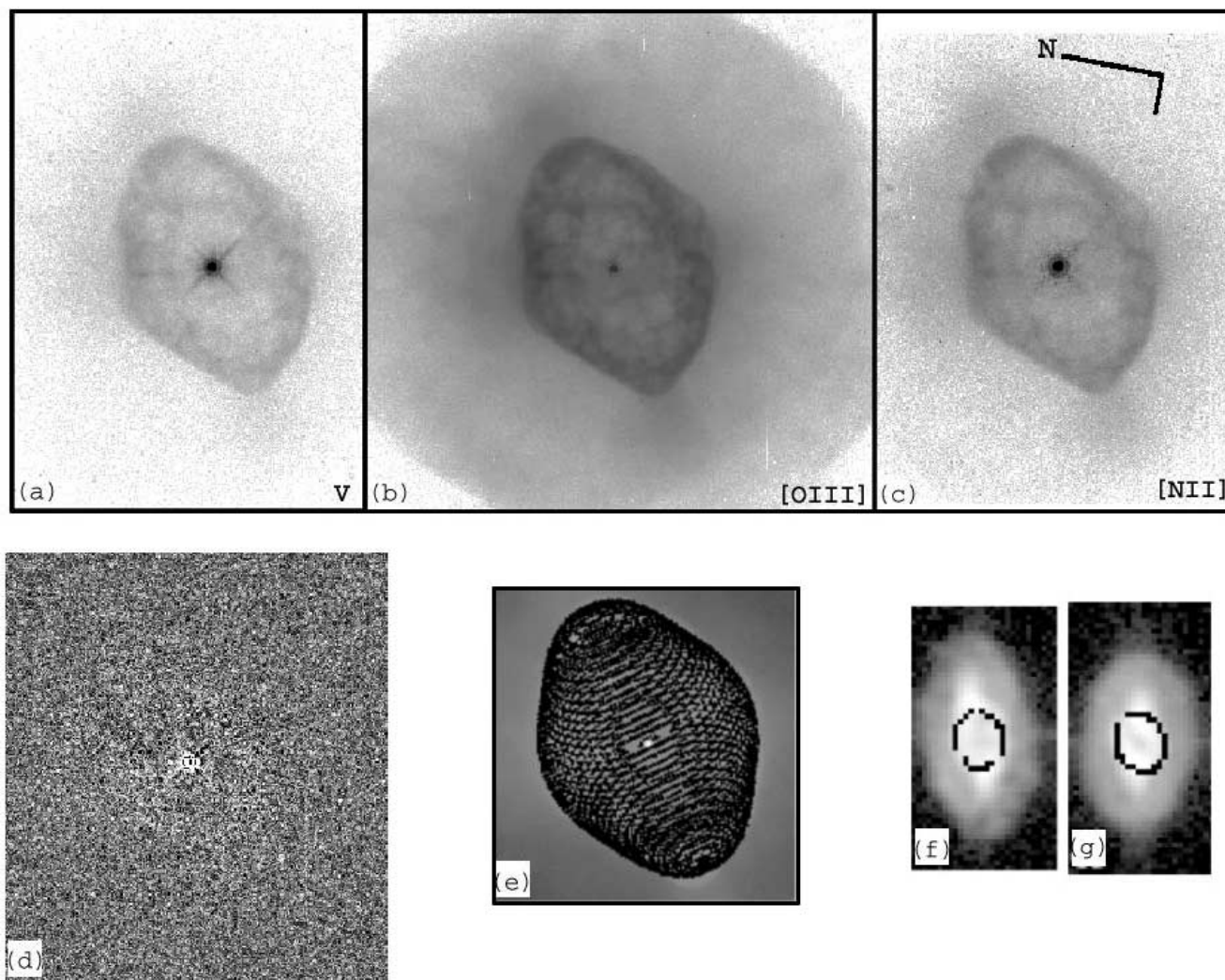


FIG. 5.—Observations of and model fits to NGC 6884: (a) original epoch 2 V -band image; (b) [O III] image; (c) [N II] image; (d) difference of the two V -band images taken 3.9 yr apart; (e) waisted ellipsoid fit to the image; (f) fit to P.A. = 220° ; (g) fit to P.A. = 310° .

so the pattern is not as clear. There is faint [N II] emission beyond the [O III] and V -band emission. This [N II] emission is somewhat clumpy, but it is not possible to determine whether the clumps have tails. There is no evidence of blow-outs or collimated outflows.

This nebula is well described as a prolate ellipsoid with axial ratio 1.5 : 1 and an inclination angle of 35° . The quite straight edges of this nebula require n to be larger than for any other nebula in this study; about 6.0 fits the nebula well.

7.2. Distance/Size Determination

The echelle data yield an expansion velocity of 7.67 km s^{-1} for this nebula, which is only marginally resolved. The V -band and the [O III] images of this nebula do not correspond well (Fig. 5). In the [O III] line, the halo is of comparable brightness with the inner core (the two regions are distinguished more by their morphologies than by a change in luminosity). It is probable that the [O III] spectroscopy is sampling the halo rather than the inner core.

As might be expected from the low expansion velocity, the expansion was too slow to be reliably detected by either the gradient method or the magnification method. However, we can place an upper limit on the expansion of

approximately 1.6 mas yr^{-1} (the smallest expansion detected in the other objects). Combining this value with the marginally resolved expansion velocity gives a lower bound of 1.0 kpc for the distance to NGC 6891. Correcting for instrumental smearing, the expansion velocity may be as low as 6.5 km s^{-1} , which slightly decreases this lower bound, giving 0.9 kpc.

8. IC 2448

8.1. Morphology

IC 2448 is an excellent target for this project. The nebula is elliptical and plain, with no complicated inner and outer structure (see Fig. 6). The lack of field stars made image alignment difficult, but the final difference image shows a high degree of symmetry, and so we are confident that the alignment is good.

The [N II] and [O III] emissions in this nebula are coincident and entirely diffuse, with no bright knots or filaments, consistent with a picture of an old, evolved nebula. The [O III] emission dominates the V -band images, as is made clear by the close correspondence in morphology between

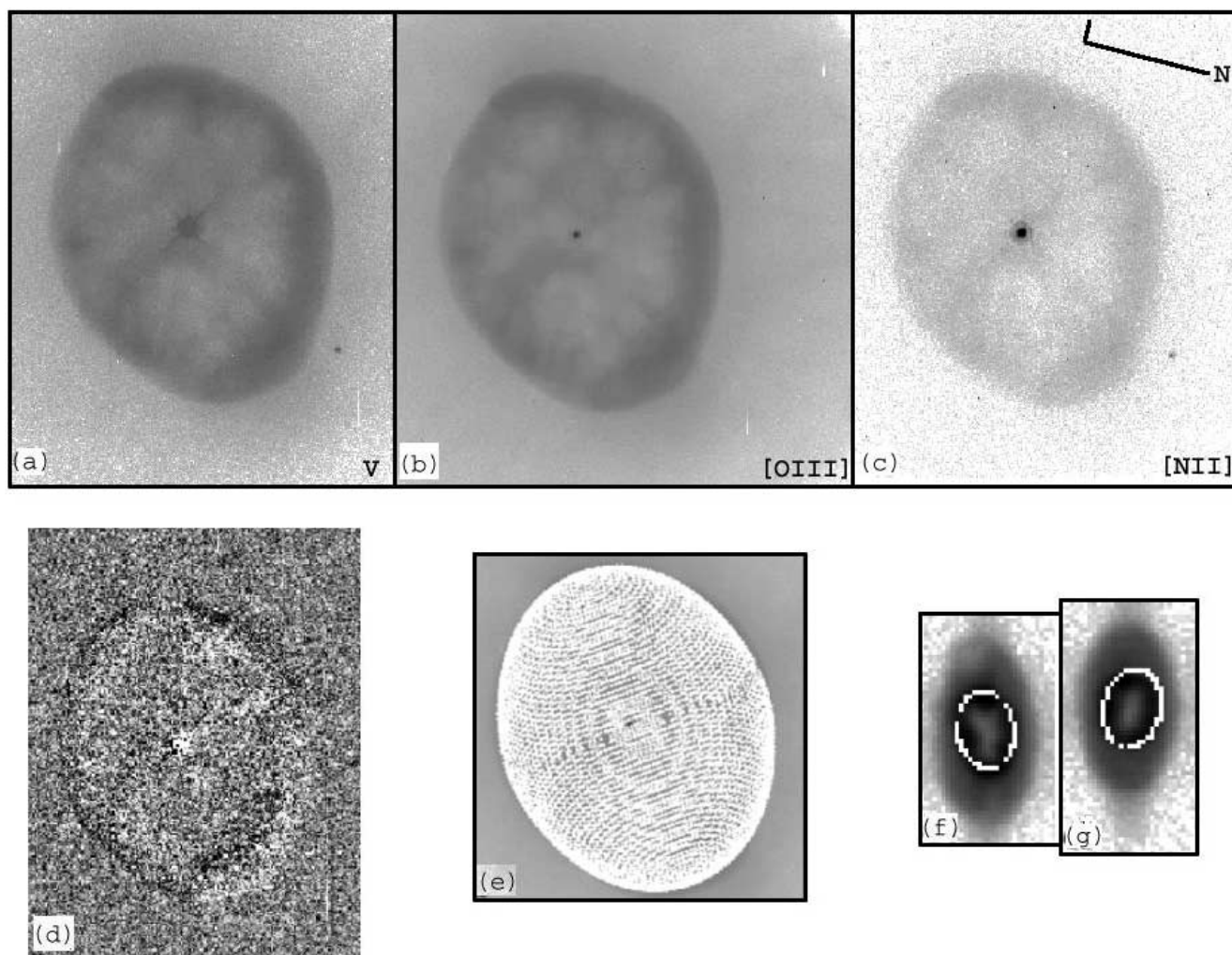


FIG. 6.—Observations of and model fits to IC 2448: (a) original epoch 2 V -band image; (b) [O III] image; (c) [N II] image; (d) difference of the two V -band images taken 4.0 yr apart; (e) waisted ellipsoid fit to the image; (f) fit to P.A. = 135° ; (g) fit to P.A. = 215° .

the two images (Fig. 6). We can be confident that the angular expansion observed in V band is a good match to the kinematic expansion observed in [O III].

The outer ring of IC 2448 appears to *compress* over time, that is, it gets thinner, with the inner radius increasing faster than the outer radius. This could be interpreted as an indication that a younger, faster wind is sweeping up material, except that the brightness of the ring does not appear to change. A second interpretation is that the nebula is old, the central star has ceased producing ionizing photons, and the nebula is beginning to fade. In the inner, denser regions, the nebula fades faster than in the outer, more diffuse regions. This interpretation is supported by the evolutionary age of the nebula, which McCarthy et al. (1990) report as 8400 yr. This nebula is very well fitted by a prolate ellipsoid with axial ratio 1.3 : 1 and an inclination angle of 25° .

8.2. Distance/Size Determination

A total of 4 yr elapsed between observations of IC 2448. The kinematic line-of-sight expansion velocity of IC 2448 is $17.9 \pm 0.3 \text{ km s}^{-1}$. Figure 6 shows the image data.

The gradient method yields an angular expansion velocity of $2.19 \pm 1.0 \text{ mas yr}^{-1}$, corresponding to a distance of $1.41 \pm 0.64 \text{ kpc}$. The magnification method gives an angular

expansion velocity of $2.25 \pm 0.6 \text{ mas yr}^{-1}$, or a distance of $1.38 \pm 0.4 \text{ kpc}$. At *HST* resolution, this nebula has no obvious variation in the proper motion with position angle.

9. CONCLUSIONS AND FUTURE WORK

Table 6 summarizes the distance determinations of the statistical methods, as well as the expansion parallax methods under consideration here. In general, there is fair agreement between the three methods, considering the large errors on the statistical distances. IC 2448 is the glaring

TABLE 6
EXPANSION PARALLAX DISTANCE DETERMINATIONS

Object	Statistical D (kpc)	Magnification D (kpc)	Gradient D (kpc)
NGC 6578.....	2.43, ^a 2.40 ^b	2.00 ± 0.5	1.63 ± 1.07
NGC 6884.....	2.57, ^a 2.108, ^a 5.4 ^b	2.20 ± 0.8	1.56 ± 0.98
IC 2448	3.10, ^b 3.20, ^a 3.95 ^c	1.38 ± 0.4	1.41 ± 0.64

^a van de Steene and Zijlstra 1994.

^b Zhang 1995.

^c Cahn et al. 1992.

exception, where the difference between the distances determined in this paper and the statistical distances is more than a factor of 2. Martin (1994) found a similar discrepancy via the extinction method. His observations put a firm upper limit of 1.5 kpc on the distance to this nebula, since the nebula is in the foreground of a cloud located between 1.5 and 2 kpc away. Our measurements are consistent with this firm upper limit, while the statistical distances are not.

Interestingly, all of the expansion parallax distances determined here are smaller than the statistical distances. However, we feel that it would be a mistake to generalize this to all nebulae. Not only is the current sample small, but it is also biased in favor of close nebulae. More distant nebulae require more time to observe an angular expansion and also would have small angular diameters; therefore, they are unlikely to be chosen for this study.

The magnification method and the gradient method are in good agreement in this study. Certainly they overlap to within the error bars. However, we believe there are systematics inherent in the magnification method that make the errors much more difficult to quantify. For example, when the nebula expands nonuniformly, determining the best magnification is quite subjective. For the cases in this paper, the nebulae expand fairly uniformly, and so these errors are small. When two different individuals perform the magnification method on these nebulae, their answers differ by at most ~ 0.001 . Operationally, this should be taken as the error in the magnification method (when propagated through the error equations, even this error is negligible compared with the error in measuring the size of the neb-

ula). In cases in which the nebula departs drastically from uniform expansion, the gradient method is more easily quantified and therefore gives more repeatable results.

We have shown that the expansion parallax method using *HST* gives distances to PNs. For nebulae that are quite similar in [O III] and *V*-band images and expand uniformly, the errors are well determined. Nonuniform expansion can cause unrecognized erroneous results, as does a discrepancy between [O III] and *V*-band images.

These results are, in general, in only fair agreement with previously determined statistical distances. This is not much of a surprise, since these statistical methods often use dubious assumptions.

Future work includes an analysis of the next 20 targets, determining their expansion parallax distances and further constraining the systematics. Derived distant-dependent properties, such as the luminosity of the nebula and central star, the density, and the mass, will be calculated in future papers. As more targets are analyzed, we will begin to develop a better idea of the distribution and density of nebulae in the galaxy, improving constraints on chemical evolution and galactic dynamics.

We would like to thank Sean Doyle for the use of his three-dimensional modeling code for IDL. Support for this work was provided by NASA through grants GO7501 and GO8390 from the Space Telescope Science Institute, which is operated by AURA, Inc., under NASA contract NAS 5-26555.

REFERENCES

- Acker, A., Fresneau, A., Pottasch, S. R., & Jasiewicz, G. 1998, *A&A*, 337, 253
 Bond, H. E., & Ciardullo, R. 1999a, *AJ*, 118, 488
 ———. 1999b, *PASP*, 111, 217
 Cahn, J. H., Kaler, J. B., & Stanghellini, L. 1992, *A&AS*, 94, 399
 Ciardullo, R., Bond, H. E., Sipior, M. S., Fullton, L. K., Zhang, C.-Y., & Schaefer, K. G. 1999, *AJ*, 118, 488
 Daub, C. T. 1982, *ApJ*, 260, 612
 Fruchter, A. S., & Hook, R. N. 2002, *PASP*, 114, 144
 Gomez, Y., Rodriguez, L. F., & Moran, J. M. 1993, *ApJ*, 416, 620
 Gutierrez-Moreno, A., Anguita, C., Loyola, P., & Moreno, H. 1999, *PASP*, 111, 1163
 Hajian, A. R., & Terzian, Y. 1996, *PASP*, 108, 419
 Hajian, A. R., Terzian, Y., & Bignell, C. 1993, *AJ*, 106, 1965
 ———. 1995, *AJ*, 109, 2600
 Harris, H. C., Dahn, C. C., Monet, D. G., & Pier, J. R. 1997, *IAUS*, 180, 40
 Iben, I., Jr. 1985, in *Mass Loss from Red Giants* (Dordrecht: Reidel), 1
 Maciel, W. J., & Pottasch, S. R. 1980, *A&A*, 88, 1
 Martin, W. 1994, *A&A*, 281, 526
 Martins, L. P., & Viegas, S. M. M. 2000, *A&A*, 361, 1121
 Masson, C. R. 1989a, *ApJ*, 336, 294
 ———. 1989b, *ApJ*, 346, 243
 McCarthy, J. K., Mould, J. R., Mendez, R. H., Kudritzki, R. P., Husfeld, D., Herrero, A., & Groth, H. G. 1990, *ApJ*, 351, 230
 O'Dell, C. R. 1962, *ApJ*, 135, 371
 Palla, F., Bachiller, R., Stanghellini, L., Tosi, M., & Galli, D. 2000, *A&A*, 355, 69
 Pottasch, S. R., & Acker, A. 1998, *A&A*, 329, L5
 Reed, D. S., Balick, B., Hajian, A. R., Klayton, T. L., Giovanardi, S., Casertano, S., Panagia, N., & Terzian, Y. 1999, *AJ*, 118, 2430 (Paper I)
 Shklovskii, I. S. 1956, *Azh*, 33, 222
 Terzian, Y. 1993, in *Planetary Nebulae*, ed. R. Weinberger & A. Acker (Dordrecht: Kluwer), 109
 van de Steene, G. C., & Zijlstra, A. A. 1994, *A&AS*, 108, 485
 Weinberger, R. 1989, *A&AS*, 78, 301
 Zhang, C.-Y. 1995, *ApJS*, 98, 659